

# Decay of the Ar $2s^{-1}$ and $2p^{-1}$ and Kr $3p^{-1}$ and $3d^{-1}$ hole states studied by photoelectron-ion coincidence spectroscopy

S. Brünken,<sup>\*</sup> Ch. Gerth,<sup>†</sup> B. Kanngießer, T. Luhmann,<sup>‡</sup> M. Richter,<sup>§</sup> and P. Zimmermann  
*Institut für Atomare Physik und Fachdidaktik, Technische Universität Berlin, Hardenbergstraße 36, D-10623 Berlin, Germany*  
 (Received 11 October 2001; published 21 March 2002)

The decay channels of the Ar  $2s^{-1}$  and  $2p^{-1}$  and Kr  $3p^{-1}$  and  $3d^{-1}$  electronic hole states have been investigated by means of photoelectron-photoion coincidence measurements following innershell ionization using synchrotron radiation. With the method of final ion-charge resolving electron spectroscopy it has become possible to disentangle different contributions to the electron spectrum and to determine the decay probabilities  $P(nl^{-1} \rightarrow n+)$  of the above-mentioned hole states ( $nl^{-1}$ ) to the final ionic charge states  $n+$ . A high correlation with threefold or even fourfold charged ions has been found in all cases. Possible decay routes, via cascade or direct double Auger processes, are discussed on the basis of energy-level schemes calculated with the Hartree-Fock method. Special emphasis is laid on the examination of the Kr  $3p^{-1}$  decay process, where the two fine-structure components ( $j = 1/2, 3/2$ ) exhibit noticeably different decay probabilities to Kr<sup>3+</sup> and Kr<sup>4+</sup> final ionic charge states.

DOI: 10.1103/PhysRevA.65.042708

PACS number(s): 32.80.Fb

## I. INTRODUCTION

The decay of inner-shell hole states in the sub-keV region is dominated by Auger transitions involving the emission of electrons with element-specific, discrete kinetic energies. Auger-electron spectroscopy, therefore, has been established as a standard analytical method [1] as well as a method for the investigation of inner-shell hole states. The creation of an inner-shell hole state in a many-electron atom is followed by a multistep cascade process, in which vacancies are transferred via different decay channels to the outer shells. Hence, for the investigation of the decay of inner-shell hole states one has to take into account additional decay channels, e.g., radiative transitions or double Auger decay involving the multiple emission of electrons with continuous energy distributions. A complex situation is thus created where electron spectroscopy alone is of limited use. Coincidence techniques provide a way to select a subset of possible transitions in order to disentangle these complex decay routes.

The photoelectron-ion coincidence technique with energy-analyzed electrons has proven to be a powerful tool for the investigation of different decay routes following inner-shell photoionization [2–7]. The initial ionic state is marked in a photoelectron-ion coincidence experiment by the energy measurement of the emitted photoelectron. The subsequent measurement of the charge state of the coincident ion then reveals the final ionic charge state of the decay route. The different ionic charge states are correlated to different decay

routes. No increase in the charge state with respect to the initial ionic state implies radiative transitions; any increase in the charge state is connected with the corresponding number of emitted Auger electrons. This way, the photoelectron-ion coincidence method relates information about the initial state obtained by electron spectroscopy to information about the final ionic charge state obtained by ion spectroscopy.

In this paper, we report on electron-ion coincidence measurements investigating the decay of the Ar  $2s^{-1}$  and  $2p^{-1}$  and Kr  $3p^{-1}$  and  $3d^{-1}$  hole states. Special emphasis is laid on the decay routes connected with 3+ and 4+ charged final ionic states, i.e., multistep and direct double Auger decays.

## II. EXPERIMENT

### A. Principle setup

The experiments were carried out at the electron storage ring BESSY I in Berlin, Germany. Monochromatic synchrotron radiation was provided by the toroidal grating monochromators HE-TGM 2 and TGM 3 for the photoionization of Ar and Kr.

Electrons emitted in the photoionization process are analyzed according to their kinetic energy by a cylindrical mirror analyzer. These electrons serve as start signals for time-of-flight (TOF) measurements of ions, in which the ions are separated by their mass-to-charge ratio. Photoions that produce stop signals in the TOF measurements are denoted as coincidence signals and registered in the coincidence spectrum. A full account of our experimental setup can be found in Ref. [6].

### B. Coincidence measurements

The relative intensities of the different ion species in a coincidence spectrum do not represent directly the correlation probabilities  $p(\epsilon, n+)$ , i.e., the probabilities for the correlation of  $n$ -fold charged photoions to electrons of the selected kinetic energy  $\epsilon$ . The following distortion effects have

<sup>\*</sup>Present address: I. Physikalisches Institut, Universität zu Köln, Zùlpicher Straße 77, D-50937 Köln, Germany.

<sup>†</sup>Present address: Deutsches Elektronen-Synchrotron DESY, Notkestraße 85, D-22603 Hamburg, Germany.

<sup>‡</sup>Present address: CANBOX AG, Cloppenburger Straße 316, D-26133 Oldenburg, Germany.

<sup>§</sup>Permanent address: PTB/BESSY, Albert-Einstein-Strasse 15, D-12489 Berlin, Germany.

to be taken into account for the determination of the correlation probabilities: (i) the occurrence of false starts and false coincidences, (ii) the dead time in the coincidence signal registration, (iii) the finite transmission of the TOF spectrometer, and (iv) the detection efficiency of the ion detector. In order to deduce the true coincidences from a coincidence spectrum, the distribution of false coincidences is measured in a reference spectrum under the same experimental conditions, where the start signals are generated periodically by a pulser with the identical start rate as in the coincidence measurement. The spectrum of true coincidences is then calculated from both the coincidence and reference spectrum whereby the above-mentioned distortion effects are taken into account; this evaluation procedure is described in detail in Ref. [8]. The transmission and detection efficiencies of the TOF spectrometer are mainly dependent on the ionic charge state leading to a discrimination of ions with a lower charge state. In order to correct the coincidence spectra for these detection distortions, the ratios of the different ion charge states were determined from the reference spectra and compared to those found in the literature [9,10] measured at the identical photon energy. The resulting correction factors were applied to the ratios of the respective ionic charge states measured in the coincidence spectra.

### C. FIRE spectroscopy

The main goal of a photoelectron-ion coincidence measurement is the determination of the probabilities  $P(nl^{-1} \rightarrow n+)$  for the decay of an inner-shell hole state  $nl^{-1}$  into the different final ionic charge states  $n+$ . Due to photoionization processes causing a continuous distribution in the electron spectra, e.g., direct double photoionization or direct double Auger decay, the correlation probabilities  $p(\epsilon, n+)$ , measured at a kinetic energy  $\epsilon$  of a specific photoelectron line, in general, deviate from the decay probabilities  $P(nl^{-1} \rightarrow n+)$  of the corresponding core hole state  $nl^{-1}$ . Various photoionization processes have been disentangled in the electron spectrum of Ar and Kr with our method of final ion-charge resolving electron (FIRE) spectroscopy. FIRE spectroscopy is an extended form of photoelectron-ion coincidence spectroscopy, where coincidence measurements are carried out for a complete electron spectrum, i.e., measurements are also performed in the energy regions between the photoelectron lines.

To demonstrate the capability of FIRE spectroscopy we have chosen the relatively weak Ar  $2s$  photoelectron line [0.25(10) Mb at 360 eV [11]], which is superimposed on a comparably large background of a continuous electron distribution. The upper part of Fig. 1 shows the  $2s$  photoelectron spectrum of Ar recorded at a photon energy of 360 eV. Background in the electron spectrum that does not originate from Ar photoionization processes has been subtracted. The results of the coincidence measurements are presented in the lower part of Fig. 1: the correlation probabilities  $p(\epsilon, n+)$  for the final ionic charge states  $1+$  to  $4+$  in the energy range  $20 \text{ eV} \leq \epsilon \leq 40 \text{ eV}$ . For each coincidence measurement at kinetic energy  $\epsilon$ , the sum  $\sum_{n=1}^4 p(\epsilon, n+)$  is normalized to 1. As a first result, the electrons in the vicinity of the

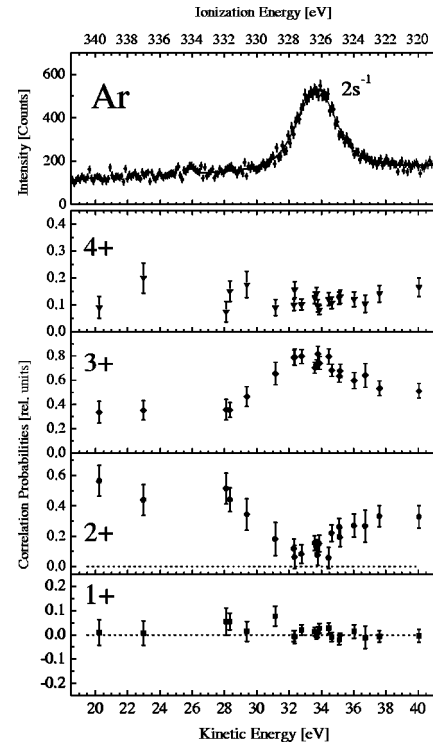


FIG. 1. Top:  $2s$  photoelectron spectrum of Ar recorded at a photon energy of 360 eV. Bottom: correlation probabilities  $p(\epsilon, n+)$  for the final ion-charge states  $\text{Ar}^{1+}$  to  $\text{Ar}^{4+}$  measured at kinetic energies  $\epsilon$ .

$2s$  emission are mainly correlated to doubly and triply charged ions, i.e.,  $\text{Ar}^{2+}$  and  $\text{Ar}^{3+}$ . However, the correlation probabilities  $p(\epsilon, 2+)$  and  $p(\epsilon, 3+)$  in the vicinity of the  $2s$  photoelectron line differ drastically from those of the adjacent continuous electron distribution. Since the  $2s$  line is superimposed on this continuous distribution, electrons originating from photoionization processes that result in this background contribute significantly to the correlation probabilities measured at kinetic energies of the  $2s$  line. Hence, for an accurate analysis of the decay probabilities  $P(2s^{-1} \rightarrow n+)$ , this contribution of the continuous electron distribution to the correlation probabilities has to be subtracted.

With the aid of the correlation probabilities obtained from the coincidence measurements, the electron spectrum can be decomposed into parts that are correlated to photoionization processes ending up in a certain final ionic charge state. Such a final ion-charge resolved electron spectrum [FIRE( $n+$ ) spectrum] can be produced by multiplying the correlation probabilities  $p(\epsilon, n+)$  for a certain charge state  $n+$  at each kinetic energy  $\epsilon$  with the corresponding signal intensity of the photoelectron spectrum. The FIRE( $n+$ ) spectra for the charge states  $1+$  to  $4+$  in the region of the  $2s$  photoelectron line have been determined by applying this method and are shown in the lower part of Fig. 2 (dots with error bars). The solid lines represent the results of fits with Voigt profiles. The upper part of Fig. 2 depicts the  $2s$  photoelectron spectrum with its decomposition into the different FIRE( $n+$ ) spectra represented by gray areas, whereby each gray shade corresponds to one charge state as shown in the lower part. Due to

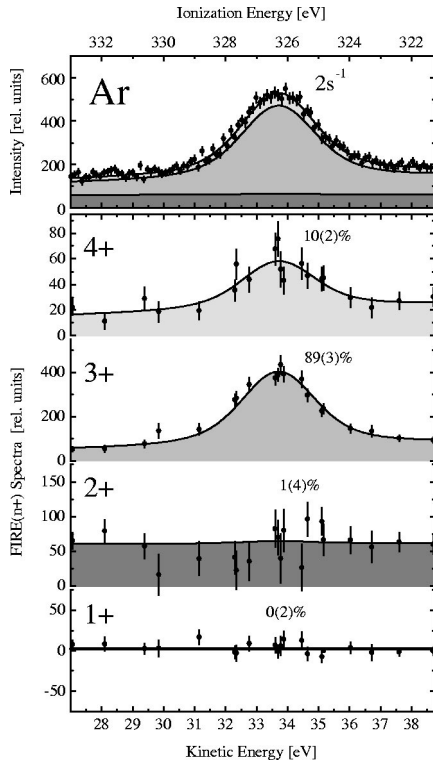


FIG. 2. Top:  $2s$  photoelectron spectrum of Ar recorded at a photon energy of 360 eV. Bottom: FIRE( $n+$ ) spectra of the charge states  $\text{Ar}^{1+}$  to  $\text{Ar}^{4+}$  (note the change of scale).

the normalization relation of the correlation probabilities, the sum of all FIRE( $n+$ ) spectra amounts to the original electron spectrum. The decay probabilities  $P(2s^{-1} \rightarrow n+)$  for the  $2s^{-1}$  core hole have been calculated from the areas of the corresponding Voigt profiles in the FIRE( $n+$ ) spectra and the results have been included in Fig. 2 (in percent). By means of this procedure, the  $2s$  photoionization process has been separated from processes leading to a continuous electron distribution, and an accurate determination of the decay probabilities became possible. A detailed description of our photoelectron-ion coincidence method and the generation of FIRE spectra can be found in Ref. [6].

### III. RESULTS AND DISCUSSION

The method of FIRE spectroscopy has been applied to study the decay probabilities for each fine-structure component of the  $\text{Ar } 2s^{-1}$  and  $2p^{-1}$  and  $\text{Kr } 3p^{-1}$  and  $3d^{-1}$  hole states.

#### A. Argon $2s^{-1}$ and $2p^{-1}$

Let us first concentrate on the decay of the  $\text{Ar } 2s^{-1}$  hole state. As described in detail above, the upper part of Fig. 2 shows the  $2s$  photoelectron spectrum of Ar together with its decomposition into the various FIRE( $n+$ ) spectra. The lower part of Fig. 2 presents the FIRE( $n+$ ) spectra for the final charge states  $1+$  to  $4+$  as well as the decay probabilities  $P(2s^{-1} \rightarrow n+)$  determined from the FIRE( $n+$ ) spectra. As can be seen from the decay probabilities, the  $2s^{-1}$  hole

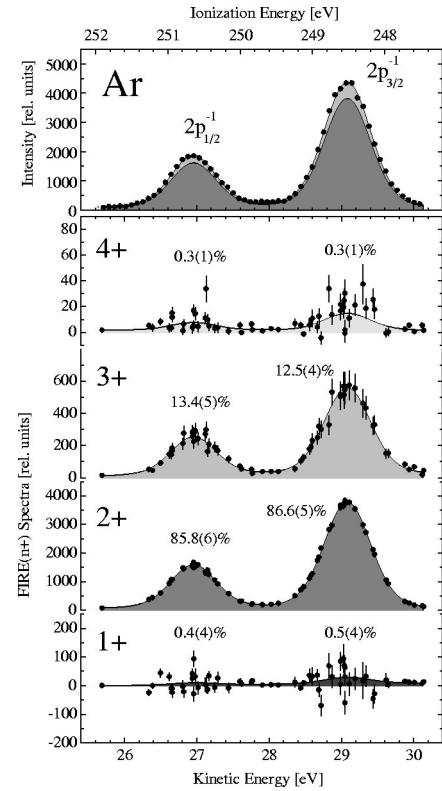


FIG. 3. Top:  $2p$  photoelectron spectrum of Ar recorded at a photon energy of 278 eV. Bottom: FIRE( $n+$ ) spectra of the charge states  $\text{Ar}^{1+}$  to  $\text{Ar}^{4+}$  (note the change of scale).

state decays predominantly with 89(3)% into  $\text{Ar}^{3+}$  final states. The probability for the decay into  $\text{Ar}^{4+}$  final states is 10(2%). The FIRE( $2+$ ) spectrum reveals a nearly continuous intensity distribution that can be related to direct double photoionization processes, and the decay probability  $P(2s^{-1} \rightarrow 2+)$  amounts to only 1(4%). As expected for shallow inner shells, the fluorescent decay connected with  $\text{Ar}^{1+}$  final states is negligible. A verification of the theoretical prediction for the  $L$ -shell fluorescence yield of 0.147% [12] is limited due to the statistical error of the measured value  $P(2s^{-1} \rightarrow 1+) = 0(2)\%$ . The  $2s^{-1}$  hole state is energetically allowed to decay into  $\text{Ar}^{1+}$  up to  $\text{Ar}^{6+}$  final ionic states. However, signals of  $\text{Ar}^{5+}$  and  $\text{Ar}^{6+}$  ions were not observed in the ion spectrum and, hence, decay routes into these final ionic states can be neglected and are not discussed further.

The  $2p$  photoelectron spectrum and the corresponding FIRE( $n+$ ) spectra are shown in Fig. 3. The photon energy was tuned to 280 eV in order to resolve the fine-structure splitting into the  $2p_{1/2}^{-1}$  and  $2p_{3/2}^{-1}$  states. From the decay probabilities included in the lower part of Fig. 3, it can be concluded that transitions into  $\text{Ar}^{2+}$  final states dominate the decay of the  $2p^{-1}$  hole states. The values for both fine-structure states are quite similar. The probability of the  $2p_{3/2}^{-1}$  state for the decay into  $\text{Ar}^{3+}$  final states of 12.5(4)% is slightly smaller than the value of 13.4(5)% for the  $2p_{1/2}^{-1}$  state at higher ionization energies. A small probability  $P(2p^{-1} \rightarrow 4+) = 0.3(1)\%$  was found for the decay into  $\text{Ar}^{4+}$  final

TABLE I. Decay probabilities  $P(2s^{-1} \rightarrow n+)$  and  $P(2p_j^{-1} \rightarrow n+)$  of Ar. Values are given in percent (%).

Hole state	Final ionic charge state			
	1+	2+	3+	4+
$2s^{-1}$	0(2)	1(4)	89(3)	10(2)
$2p_{1/2}^{-1}$	0.4(4)	85.8(6)	13.4(5)	0.3(1)
$2p_{3/2}^{-1}$	0.5(4)	86.6(5)	12.5(4)	0.3(1)

states. As in the case of the  $2s^{-1}$  hole state, radiative decay of the  $2p^{-1}$  states into  $\text{Ar}^{1+}$  final states is negligible. Again, the upper limits of the measured decay probabilities of  $0.4\% \pm 0.4\%$  ( $2p_{1/2}^{-1}$ ) and  $0.5\% \pm 0.4\%$  ( $2p_{3/2}^{-1}$ ) due to the statistical error are much larger than the theoretical prediction [12]. The measured decay probabilities  $P(2s^{-1} \rightarrow n+)$  and  $P(2p^{-1} \rightarrow n+)$  of Ar are summarized in Table I.

For the interpretation of the decay probabilities, single-configuration Hartree-Fock (SC-HF) calculations for various energy levels of  $\text{Ar}^{1+}$  to  $\text{Ar}^{4+}$  in the energy range 0–350 eV were carried out with the use of the COWAN code [13]. The energy-level scheme shown in Fig. 4 summarizes the results and represents a simplified picture of the states relevant for the decay of the  $2s^{-1}$  and  $2p^{-1}$  hole states. Arrows indicate main decay routes.

From the energy-level scheme in Fig. 4, it can be seen that the main decay routes of the  $2s^{-1}$  hole state are cascade transitions to  $\text{Ar}^{3+}$  final states:  $\text{Ar}^{1+}2s^{-1} \rightarrow \text{Ar}^{2+}2p^{-1}(3s,3p)^{-1} \rightarrow \text{Ar}^{3+}(3s,3p)^{-3}$ . Here, the notation  $(n_1l_1, n_2l_2)^{-x}$  includes all possible combinations of  $x$  hole states in the subshells  $n_1l_1$  and  $n_2l_2$ , e.g., the expression  $(3s,3p)^{-3}$  comprises the hole states  $3s^{-2}3p^{-1}$ ,  $3s^{-1}3p^{-2}$ , and  $3p^{-3}$ . This two-step decay gives rise to discrete Auger lines in the electron spectrum. The  $L_1L_{2,3}M$  Auger lines

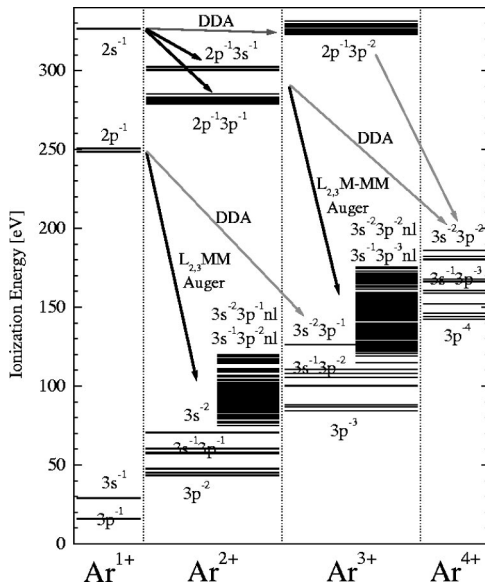


FIG. 4. Energy-level scheme of Ar calculated with the HF method in single-configuration approximation. Energy positions of the  $\text{Ar}^{2+} 3s^{-2}$ ,  $3s^{-1}3p^{-1}$ , and  $3p^{-2}$  levels have been derived from Ref. [16].

stemming from the first step of the decay occur at kinetic energies between 28 eV and 50 eV [14]. This Auger decay mainly determines the natural width of the  $2s$  photoelectron line of 2.25(5) eV [15]. The  $L_{2,3}M-MM$  Auger lines of the second step are superimposed on the  $L_{2,3}MM$  Auger lines resulting from the decay of the  $2p^{-1}$  hole states. These Auger lines have been studied intensely by electron spectroscopy [16,17] and by electron-ion coincidence spectroscopy after  $K$ -shell ionization [18,19].

Due to the large overlap of  $2s$  and  $2p$  wave functions in the  $L$  shell, the transition probabilities of the Auger decay  $\text{Ar}^{1+}2s^{-1} \rightarrow \text{Ar}^{2+}2p^{-1}(3s,3p)^{-1}$  as the first step of the cascade transitions are apparently much larger than those of the Auger transitions creating two holes in the  $M$  shell  $\text{Ar}^{1+}2s^{-1} \rightarrow \text{Ar}^{2+}(3s,3p)^{-2}$ . The latter transitions are connected with the production of  $\text{Ar}^{2+}$  final states and would show up as  $\text{Ar}^{2+}$  signals. From the small decay probability  $P(2s^{-1} \rightarrow 2+) = 1(4)\%$ , it can be concluded that these transitions contribute only weakly to the decay of the  $2s^{-1}$  hole state.

It is interesting to consider the decay routes that are connected with the production of  $\text{Ar}^{4+}$ . From the energy-level scheme in Fig. 4 one can deduce that one possible decay route corresponds to cascade transitions for which the first step  $\text{Ar}^{1+}2s^{-1} \rightarrow \text{Ar}^{2+}2p^{-1}(3s,3p)^{-1}$  is the same as for the main decay into  $\text{Ar}^{3+}$  final states. However, the second step of the decay  $\text{Ar}^{2+}2p^{-1}(3s,3p)^{-1} \rightarrow \text{Ar}^{3+}(3s,3p)^{-4}nl$  comprises Auger decays with an additional shake up leading to  $\text{Ar}^{3+}3s^{-1}3p^{-3}nl$  or  $\text{Ar}^{3+}3s^{-2}3p^{-2}nl$  states that subsequently decay to  $\text{Ar}^{4+}3p^{-4}$  or  $3s^{-1}3p^{-3}$ . Another possibility for the production of  $\text{Ar}^{4+}$  are direct double Auger (DDA) transitions in the second step of the cascade such as  $\text{Ar}^{2+}2p^{-1}(3s,3p)^{-1} \rightarrow \text{Ar}^{4+}(3s,3p)^{-4}$ .

The  $2p_{1/2}^{-1}$  and  $2p_{3/2}^{-1}$  states decay predominantly via  $L_{2,3}MM$  Auger transitions  $\text{Ar}^{1+}2p^{-1} \rightarrow \text{Ar}^{2+}(3s,3p)^{-2}$  leading to  $\text{Ar}^{2+}$  final ionic states. The decay into  $\text{Ar}^{3+}$  final ionic states can be explained by cascade transitions via intermediate shake-up states  $\text{Ar}^{1+}2p^{-1} \rightarrow \text{Ar}^{2+}(3s,3p)^{-3}nl \rightarrow \text{Ar}^{3+}(3s,3p)^{-3}$  or by direct double Auger decay  $\text{Ar}^{1+}2p^{-1} \rightarrow \text{Ar}^{3+}(3s,3p)^{-3}$ .

The only calculation on the decay of the  $\text{Ar}2s^{-1}$  and  $2p^{-1}$  hole states we found in the literature has been performed by Kochur *et al.* [20], who applied a straightforward HF model to construct deexcitation trees following the creation of the hole states. As the authors already pointed out for the shallow hole states, the calculations underestimate the decay probabilities for the ions with higher charge states ( $\text{Ar}^{3+}$  and  $\text{Ar}^{4+}$ ). Deviations from the measured values are most pronounced for the decay probability of the  $2p^{-1}$  hole state: the measured mean value of  $P(2p^{-1} \rightarrow 3+) = 13\%$  cannot be reproduced by the calculation, which yields a value of 0.8%.

## B. Krypton $3p^{-1}$ and $3d^{-1}$

In the following we discuss the decay of the  $\text{Kr}3p^{-1}$  and  $3d^{-1}$  hole states. The  $3p$  and  $3d$  photoelectron and FIRE( $n+$ ) spectra are shown in Figs. 5 and 6, respectively. As in the case of the  $\text{Ar}2s^{-1}$  and  $2p^{-1}$  hole states, radiative

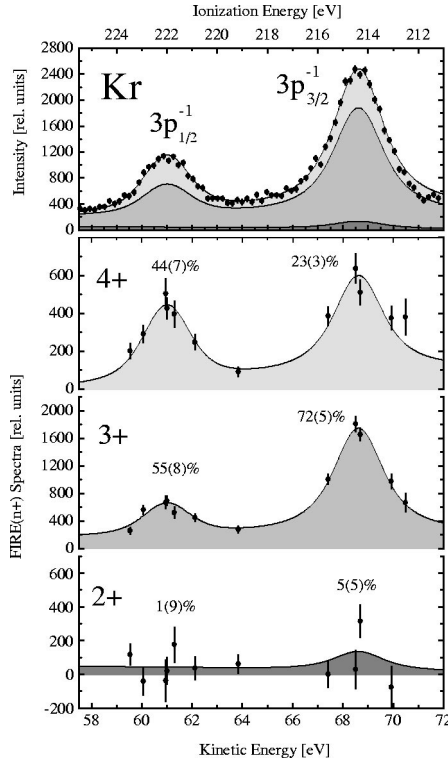


FIG. 5. Top:  $3p$  photoelectron spectrum of Kr recorded at a photon energy of 283 eV. Bottom: FIRE( $n+$ ) spectra of the charge states  $\text{Kr}^{2+}$  to  $\text{Kr}^{4+}$  (note the change of scale).

decay of the  $3p^{-1}$  and  $3d^{-1}$  hole states into  $\text{Kr}^{1+}$  final ionic charge states has been found to be negligible ( $<1\%$ ). In order to reduce the statistical error for the charge states other than  $1+$ ,  $\text{Kr}^{1+}$  has been omitted from the final evaluation procedure, and the FIRE( $1+$ ) spectra are not shown. For the  $3p^{-1}$  hole states, the decay into  $\text{Kr}^{5+}$  and  $\text{Kr}^{6+}$  is energetically allowed but has also been found to be negligible ( $<0.1\%$ ) and is not discussed further. The decay probabilities  $P(3d_j^{-1} \rightarrow n+)$  and  $P(3p_j^{-1} \rightarrow n+)$  of each fine-structure component, determined from the areas of the Voigt profiles, have been included in Figs. 5 and 6 and are summarized in Table II.

The  $3p$  spectrum of Fig. 5 was recorded at a photon energy of 284 eV, i.e., well above the  $3p$  ionization energies of 214.6 eV ( $3p_{3/2}^{-1}$ ) and 221.8 eV ( $3p_{1/2}^{-1}$ ) [21]. The most striking feature of the  $3p$  FIRE( $3+$ ) and FIRE( $4+$ ) spectra is the remarkable difference of the relative intensities for the  $3p_{1/2}^{-1}$  and  $3p_{3/2}^{-1}$  fine-structure states. As a result, the decay probability  $P(3p_{1/2}^{-1} \rightarrow 4+) = 44(7)\%$  is considerably larger than  $P(3p_{3/2}^{-1} \rightarrow 4+) = 23(3)\%$ . Consequently, the probability for the decay into  $\text{Kr}^{3+}$  final ionic states also differs significantly: 55(8)% for  $3p_{1/2}^{-1}$  and 72(5)% for  $3p_{3/2}^{-1}$ . Decay routes leading to  $\text{Kr}^{2+}$  final ionic states occur with a probability less than 10% within the error limit. For the  $3d$  spectrum, the photon energy was tuned to 116 eV. The  $3d_{3/2}^{-1}$  and  $3d_{5/2}^{-1}$  hole states decay predominantly into  $\text{Kr}^{2+}$  final ionic states with about 70% probability. The probability for the decay into  $\text{Kr}^{3+}$  final ionic states is about 30% for both fine-structure states.

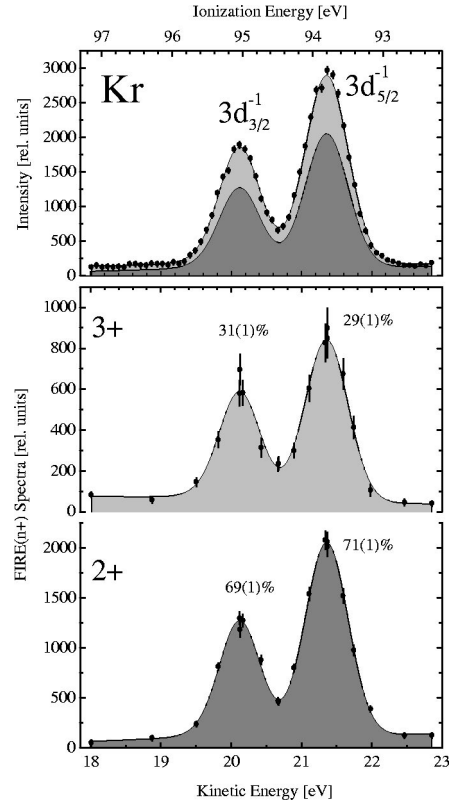


FIG. 6. Top:  $3d$  photoelectron spectrum of Kr recorded at a photon energy of 115.2 eV. Bottom: FIRE( $n+$ ) spectra of the charge states  $\text{Kr}^{2+}$  and  $\text{Kr}^{3+}$  (note the change of scale).

For the discussion of possible decay routes, we performed SC-HF calculations with the COWAN code [13] for the relevant energy levels of  $\text{Kr}^{1+}$  to  $\text{Kr}^{4+}$ . Figure 7 gives a simplified picture of the level scheme for ionization energies in the range 0–240 eV. Arrows indicate main decay routes.

In comparison to the energy-level scheme of Ar, the level structure of Kr shown in Fig. 7 exhibits distinct differences that manifest themselves in the different experimental results for the Ar and Kr FIRE( $n+$ ) spectra with respect to the higher charge states. These differences are the greater abundance of levels associated with the extra  $3d$  shell in krypton and correlation effects of the hole states with relevant levels of the next higher charge state. This is most obvious for the  $\text{Ar}^{1+} 2p^{-1}$  states and the analogous  $\text{Kr}^{1+} 3p^{-1}$  states. The latter overlap considerably with the nearby  $\text{Kr}^{2+} 3d^{-2}$  states, giving rise to strong correlation effects. These strong correlations between these states and their influence on the

TABLE II. Decay probabilities  $P(3p_j^{-1} \rightarrow n+)$  and  $P(3d_j^{-1} \rightarrow n+)$  of Kr. Values are given in percent (%).

Hole state	Final ionic charge state			
	1+	2+	3+	4+
$3p_{1/2}^{-1}$	$<1$	1(9)	55(8)	44(7)
$3p_{3/2}^{-1}$	$<1$	5(5)	72(5)	23(3)
$3d_{3/2}^{-1}$	$<1$	69(1)	31(1)	
$3d_{5/2}^{-1}$	$<1$	71(1)	29(1)	

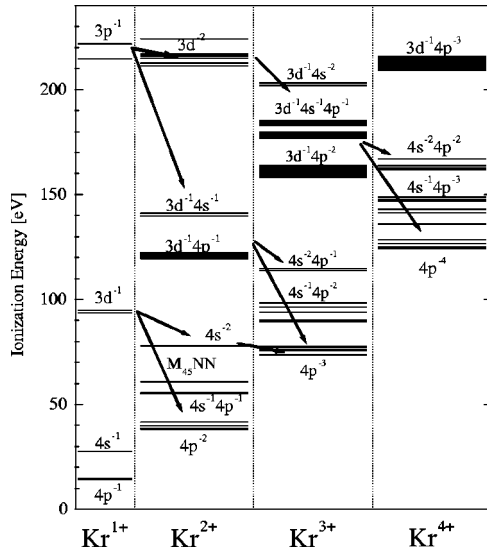


FIG. 7. Energy-level scheme of Kr calculated with the HF method in single-configuration approximation. Energy positions of  $\text{Kr}^{2+} 4s^{-2}$ ,  $4s^{-1}4p^{-1}$ , and  $4p^{-2}$  levels have been derived from Ref. [25].

$3p$  photoelectron spectrum have been observed experimentally by Svensson *et al.* [22,23] and discussed theoretically by Ohno and Wendin [24]. Due to the large overlap of the  $3p$  and  $3d$  wave functions there are strong super-Coster-Kronig (SCK) transitions  $\text{Kr}^{1+}3p^{-1} \rightarrow \text{Kr}^{2+}3d^{-2}$ . The subsequent cascade transitions  $\text{Kr}^{2+}3d^{-2} \rightarrow \text{Kr}^{3+}3d^{-1}(4s,4p)^{-2} \rightarrow \text{Kr}^{4+}(4s,4p)^{-4}$  are responsible for the relatively large number of decays ending up in  $\text{Kr}^{4+}$  final ionic states. Due to the relatively large spin-orbit splitting of the fine-structure components  $3p_{1/2}^{-1}$  and  $3p_{3/2}^{-1}$  that amounts to 8 eV, a larger number of energetically allowed  $3p$ - $3d$  SCK transitions are available for the  $3p_{1/2}^{-1}$  state. This may explain the significantly larger decay probability  $P(3p_{1/2}^{-1} \rightarrow 4+)$  of 44(7)% for the  $3p_{1/2}^{-1}$  state compared to 23(3)% for the  $3p_{3/2}^{-1}$  state. Various decay routes into  $\text{Kr}^{3+}$  final ionic states are available for the  $3p^{-1}$  states. Here, the two-step decays via  $\text{Kr}^{1+}3p^{-1} \rightarrow \text{Kr}^{2+}3d^{-1}(4s,4p)^{-1} \rightarrow \text{Kr}^{3+}(4s,4p)^{-3}$  seem to be the most favorable decay channels that lead to decay probabilities of 72(5)% for the  $3p_{3/2}^{-1}$  state and 55(8)% for the the  $3p_{1/2}^{-1}$  state. As regards the decay probability  $P(3p^{-1} \rightarrow 2+)$ , Auger decays into  $(4s,4p)^{-2}$  final states are negligible.

The  $3d_{3/2}^{-1}$  and  $3d_{5/2}^{-1}$  states decay predominantly by about 70% into  $\text{Kr}^{2+}$  final ionic states, most likely by Auger decay into the final states  $4s^{-1}4p^{-1}$  and  $4p^{-2}$ . This is corroborated by the high intensity of the corresponding  $M_{4,5}NN$  Auger lines [25,26] in the electron spectrum. In contrast to the  $\text{Ar}^{1+}2p^{-1} \rightarrow 3s^{-2}$  transitions leading to  $\text{Ar}^{2+}$  final ionic states, the  $\text{Kr}4s^{-2}$  states are located above the  $3+$  threshold and, thus, the  $3d^{-1} \rightarrow 4s^{-2}$  transitions decay further in a subsequent step into  $\text{Kr}^{3+}$  final ionic states. The decay probabilities  $P(3d_{3/2}^{-1} \rightarrow 3+) = 31(1)\%$  and  $P(3d_{5/2}^{-1} \rightarrow 3+) = 29(1)\%$  for the double Auger decay deviate from earlier results that were also obtained in a photoelectron-ion coinci-

dence experiment performed by Shigemasa *et al.* [2]. They reported on an intensity ratio for  $\text{Kr}^{3+}$  to  $\text{Kr}^{2+}$  of 0.330(5) when measured in coincidence with  $3d$  electrons, which corresponds to a decay probability  $P(3d^{-1} \rightarrow 3+) = 24.8(3)\%$ . This value is smaller than our mean value  $P(3d^{-1} \rightarrow 3+) = 30(1)\%$ , taking into account the branching ratio of  $3d_{5/2}^{-1} : 3d_{3/2}^{-1} = 1.55:1$  [27].

No theoretical predictions have been reported in the literature. As in the case of Ar, there only exist HF calculations by Kochur *et al.* [20] that do not predict satisfying results for shallow hole states. The calculated probabilities for the decay of the  $3d^{-1}$  hole states into  $\text{Kr}^{3+}$  final ionic states amount only to 1.2% and for the decay of both fine-structure components  $3p_{1/2}^{-1}$  and  $3p_{3/2}^{-1}$  into  $\text{Kr}^{4+}$  final ionic states only to 3%.

#### IV. SUMMARY

The decay of the  $\text{Ar} 2p^{-1}$  and  $2s^{-1}$  and the  $\text{Kr} 3d^{-1}$  and  $3p^{-1}$  hole states has been investigated by means of photoelectron-ion coincidence spectroscopy and possible decay routes have been discussed on the basis of energy-level schemes calculated with the SC-HF method. By applying the method of FIRE spectroscopy we have been able to separate discrete and continuous photoionization processes in the electron spectrum and to determine the probabilities for the decay of the above-mentioned hole states into the various final ionic charge states. It has been demonstrated that FIRE spectroscopy may be applied successfully to extremely weak photoelectron lines such as the Ar  $2s$  line even when superimposed on a comparably large background of continuous processes.

Fluorescence decay is negligible for all investigated hole states and the electronic decay is by far the most dominant process. A high correlation with threefold or even fourfold charged ions has been found for all hole states. Double Auger decay into  $3+$  final ionic states contributes considerably to the decay process of the  $\text{Ar} 2p^{-1}$  (13%) and  $\text{Kr} 3d^{-1}$  (30%) hole states. The  $\text{Ar} 2s^{-1}$  hole state and the  $\text{Kr} 3p^{-1}$  hole states decay mainly into  $3+$  final ionic states. The decay probabilities of the fine-structure components of the  $3p^{-1}$  hole states were found to show remarkable differences. This could be explained by the considerable overlap of these states with the  $\text{Kr}^{2+} 3d^{-2}$  levels, which open intense decay channels to  $\text{Kr}^{4+}$  final ionic states. Hence, the probability for the decay into  $\text{Kr}^{4+}$  final ionic states increases drastically for the  $3p_{1/2}^{-1}$  state at higher ionization energies. Theoretical predictions [20] strongly underestimate the decay into higher charged ions for shallow hole states. Hence, there is a substantial need for more elaborate calculations for the processes involved in the decay into higher charge states.

#### ACKNOWLEDGMENTS

The authors express their thanks to the staff at BESSY for their assistance. Financial support of the Deutsche Forschungsgemeinschaft DFG (Zi183/11-2) is greatly appreciated.

- [1] Electron Spectroscopy for Chemical Analysis (ESCA); for a review see, e.g., *Spectroscopy*, edited by B.P. Straughan and S. Walker (Wiley, New York, 1976), Vol. III.
- [2] E. Shigemasa, T. Koizumi, Y. Itoh, T. Hayaishi, K. Okuno, A. Danjo, and Y. Sato, *Rev. Sci. Instrum.* **63**, 1505 (1992).
- [3] B. Kämmerling, B. Krässig, and V. Schmidt, *J. Phys. B* **25**, 3621 (1992).
- [4] S. Baier, G. Gottschalk, T. Kerkau, T. Luhmann, M. Martins, M. Richter, G. Snell, and P. Zimmermann, *Phys. Rev. Lett.* **72**, 2847 (1994).
- [5] T. Luhmann, Ch. Gerth, M. Martins, M. Richter, and P. Zimmermann, *Phys. Rev. Lett.* **76**, 4320 (1996).
- [6] T. Luhmann, Ch. Gerth, M. Groen, M. Martins, B. Obst, M. Richter, and P. Zimmermann, *Phys. Rev. A* **57**, 282 (1998).
- [7] B. Kanngießler, M. Jainz, S. Brünken, W. Benten, Ch. Gerth, K. Godehusen, K. Tiedtke, P. van Kampen, A. Tutay, and P. Zimmermann, *Phys. Rev. A* **62**, 014702 (2000).
- [8] T. Luhmann, *Rev. Sci. Instrum.* **68**, 2347 (1997).
- [9] D.M.P. Holland, K. Codling, J.B. West, and G.V. Marr, *J. Phys. B* **12**, 2465 (1979).
- [10] F. von Busch, U. Ankerhold, S. Dress, and B. Esser, *J. Phys. B* **29**, 5343 (1996).
- [11] M. Kutzner, Q. Shamblin, S.E. Vance, and D. Winn, *Phys. Rev. A* **55**, 248 (1997).
- [12] John H. Hubbell, Report No. NISTIR 89-4144, 1989 (unpublished).
- [13] R.D. Cowan, *The Theory of Atomic Structure and Spectra* (University of California Press, Berkeley, 1981).
- [14] T. Kylli, J. Karvonen, H. Aksela, A. Kivimäki, S. Aksela, R. Camilloni, L. Avaldi, M. Coreno, M. de Simone, R. Richter, K.C. Prince, and S. Stranges, *Phys. Rev. A* **59**, 4071 (1999).
- [15] P. Glans, R.E. LaVilla, M. Ohno, S. Svensson, G. Bray, N. Wassdahl, and J. Nordgren, *Phys. Rev. A* **47**, 1539 (1993).
- [16] L.O. Werme, T. Bergmark, and K. Siegbahn, *Phys. Scr.* **8**, 149 (1973).
- [17] W. Mehlhorn, *Z. Phys.* **160**, 247 (1960); T. Kondow, T. Kawai, K. Kunimori, T. Onishi, and K. Tamaru, *J. Phys. B* **6**, L156 (1973); D. Ridder, J. Dieringer, and N. Stolterfoht, *ibid.* **9**, L307 (1976); K. Helenelund, S. Hedman, L. Asplund, U. Gelius, and K. Siegbahn, *Phys. Scr.* **27**, 245 (1983).
- [18] U. Alkemper, J. Doppelfeld, and F. von Busch, *Phys. Rev. A* **56**, 2741 (1997).
- [19] F. von Busch, U. Kuetgens, J. Doppelfeld, and S. Fritzsche, *Phys. Rev. A* **59**, 2030 (1999).
- [20] A.G. Kochur, V.L. Sukhorukov, I.D. Petrov, and Ph.V. Demekhin, *J. Phys. B* **28**, 387 (1995).
- [21] H. Siegbahn and L. Karlsson, in *Photoelectron Spectroscopy*, edited by W. Mehlhorn, *Corpuscles and Radiation in Matter*, Encyclopedia of Physics Vol. XXXI (Springer-Verlag, Berlin, 1982), p. 320.
- [22] S. Svensson, N. Mårtensson, E. Basilier, P.Å. Malmquist, U. Gelius, and K. Siegbahn, *Phys. Scr.* **14**, 141 (1976).
- [23] S. Svensson, B. Eriksson, N. Mårtensson, G. Wendin, U. Gelius, *J. Electron Spectrosc. Relat. Phenom.* **47**, 327 (1988).
- [24] M. Ohno and G. Wendin, *J. Phys. B* **11**, 1557 (1977).
- [25] L.O. Werme, T. Bergmark, and K. Siegbahn, *Phys. Scr.* **6**, 141 (1972).
- [26] W. Mehlhorn, *Z. Phys.* **165**, 21 (1965); H. Aksela, S. Aksela, and H. Pulkkinen, *Phys. Rev. A* **30**, 2456 (1984); D.W. Lindle, P.A. Heimann, T.A. Ferrett, P.H. Kobrin, C.M. Truesdale, U. Becker, H.G. Kerkhoff, and D.A. Shirley, *ibid.* **33**, 319 (1986).
- [27] S. Aksela, K.H. Tan, G.M. Bancroft, H. Aksela, B.W. Yates, and L.L. Coatsworth, *Phys. Rev. A* **32**, 1219 (1985).